

# Super-Fermi Acceleration in Multiscale MHD Reconnection

Stephen Majeski\* and Hantao Ji†

*Department of Astrophysical Sciences*

*Peyton Hall, 4 Ivy Lane*

*Princeton University, Princeton, NJ 08544*

(Dated: October 25, 2022)

We investigate the Fermi acceleration of charged particles in 2D MHD anti-parallel plasmoid reconnection, finding a drastic enhancement in energization rate  $\dot{\epsilon}$  over a standard Fermi model of  $\dot{\epsilon} \sim \epsilon$ . The shrinking particle orbit width around a magnetic island due to  $\vec{E} \times \vec{B}$  drift produces a  $\dot{\epsilon}_{\parallel} \sim \epsilon_{\parallel}^{1+1/2\chi}$  power law with  $\chi \sim 0.75$ . The increase in the maximum possible energy gain of a particle within a plasmoid due to the enhanced efficiency increases with the plasmoid size, and is by multiple factors of 10 in the case of solar flares and much more for larger plasmas. Including effects of the non-constant  $\vec{E} \times \vec{B}$  drift rates leads to further variation of power law indices from  $\gtrsim 2$  to  $\lesssim 1$ , decreasing with plasmoid size at the time of injection.

*Introduction.*—Energy conversion in magnetic reconnection is pivotal to understanding reconnection’s role throughout the Universe [1–3]. In solar flares, estimates have found as much as half of electrons being energized to non-thermal energies [4, 5]. Moreover, within the solar wind and the earth’s magnetotail, electron acceleration and power law energy spectra are often found associated with plasmoids and compressing or merging flux ropes [6–10]. Recent years have seen considerable effort to explain these observations, focusing on three leading mechanisms during reconnection: direct acceleration by reconnection electric field [11–13] or by localized instances of magnetic field-aligned electric fields [14], betatron acceleration due to field compression while conserving particle magnetic moments [15–17], and Fermi acceleration by “kicks” from the motional electric field within islands [18–21]. Fermi acceleration operates primarily in multiscale, or plasmoid, reconnection which is thought to be pervasive from solar flares to magnetospheric substorms to accretion disks [22–25]. In these environments, it takes place within the large volume of magnetic islands which pervade plasmoid-unstable current sheets [26]. A unique characteristic of Fermi acceleration which makes it particularly promising for explaining power law distributions, is that the acceleration rate is itself a power law in energy [18]. This has led to simulations finding Fermi-generated power law distributions over a range of Lundquist numbers, Lorentz factors, guide fields, and more [27, 28].

Analytical estimates of Fermi acceleration are frequently based off of the seminal work of Drake et al, which found that the particle acceleration rate is linear in the particle energy,  $\dot{\epsilon} \sim \epsilon$  [18] (in what follows we will refer to acceleration rate power law indices with  $p$ , *i.e.*  $\dot{\epsilon} \sim \epsilon^p$ ). Other approaches have similarly described Fermi acceleration in more MHD-like plasmoid mergers via conservation of the bounce invariant  $J_{\parallel}$  [17, 21].

Building off of these concepts, energetic particle spectral indices over a range of values larger than 1 have been explained through a combination of Fermi acceleration, various drifts, and particle-loss processes [20, 26]. Efforts have also been made to implement the kinetic physics of Fermi acceleration without resolving small scales [29]. Unfortunately, most *analytical* particle acceleration studies stem from kinetic simulations which are computationally limited in the scale separation between large MHD magnetic islands and the Larmor radius ( $\rho_L$ ) of accelerating particles. Yet many astrophysical systems showing promise as a source for energetic particles are deep within the MHD regime [2, 30]. Such lack of scale separation leads to difficulty in capturing effects like the conservation of adiabatic invariants, increasing loss rates from magnetic islands through pitch-angle scattering [31, 32]. Additionally, for lower energy but still weakly collisional particles, their bounce motion may not be fast enough to assume conservation of  $J_{\parallel}$ . We therefore propose a new model of Fermi-like acceleration in 2D MHD anti-parallel reconnection, finding that enhanced particle confinement to compressing magnetic field lines yields an  $\mathcal{O}(1)$  correction to the linear Fermi power law index  $p = 1$ .

*Linear Fermi acceleration.*—Consider a plasmoid embedded in a current sheet undergoing 2D anti-parallel MHD reconnection. Away from the x-point, the dominant electric field component is the out-of-plane motional field which drives the “E cross B” drift  $\vec{u}_E = c\vec{E} \times \vec{B}/B^2$  [33]. If a magnetized particle within a plasmoid is to gain energy, it must experience net motion along this electric field, in this case via guiding center drift. The only drift in this circumstance satisfying this constraint is the curvature drift  $\vec{v}_C$  (given our assumptions, drifts arising from time dependence can be ignored due to the slow nature of the the MHD background). Figure 1 shows the process of Fermi acceleration in such a setup.

As a magnetized,  $\mu = mv_{\perp}^2/2B$  conserving particle travels along a field line within the plasmoid, it crosses the narrow region of thickness  $\delta$  nearest to the neighboring x-point where  $\vec{E}$  and  $\vec{v}_C$  are both aligned and large. This increases the parallel energy according to

\* smajeski@princeton.edu

† Also at Princeton Plasma Physics Laboratory

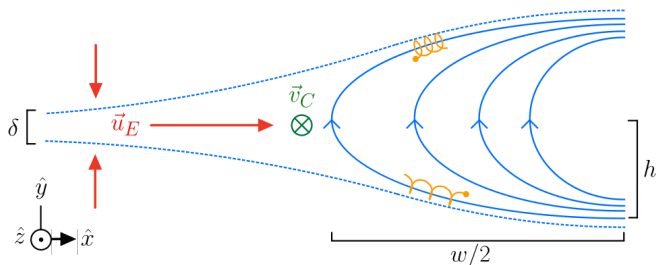


FIG. 1: Diagram of Fermi acceleration process. Blue lines represent the magnetic field (separatrix dashed), and the curvature drift is given for a positively charged particle.

$\dot{\varepsilon}_{\parallel} = 2q\vec{E} \cdot \vec{v}_C/m$ , where  $\varepsilon_{\parallel} \doteq v_{\parallel}^2$ , and

$$\vec{v}_C = \frac{m\varepsilon_{\parallel}}{qB} \hat{b} \times (\hat{b} \cdot \nabla \hat{b}) \approx -\frac{2m\varepsilon_{\parallel}}{\delta qB} \hat{z}. \quad (1)$$

The total energy imparted in this instant is then  $\dot{\varepsilon}_{\parallel} \delta / \sqrt{\varepsilon_{\parallel}} \approx 4\langle u_E \rangle_{\delta} \sqrt{\varepsilon_{\parallel}}$ , with  $\langle \rangle_{\delta}$  representing the average over the narrow layer  $\delta$ . We have also used  $|u_E| = |E/B|$ . This process occurs once every island transit time  $\Delta t_w \approx w/\sqrt{\varepsilon_{\parallel}}$ , yielding the linear Fermi acceleration rate:

$$\left( \frac{d\varepsilon_{\parallel}}{dt} \right)_F \approx 4\langle u_E \rangle_{\delta} \frac{\varepsilon_{\parallel}}{w}. \quad (2)$$

This expression is identical in appearance to that of Drake et al, with key differences in meaning [18]. The assumptions under which this equation was derived are MHD without a guide field, not kinetic, meaning no  $E_{\parallel}$  or Hall magnetic field component is present. Equation (2) has the appearance of being linear in energy, however we will show that during a particle's acceleration  $\langle u_E \rangle_{\delta}$  and  $w$  are not constant, leading to deviation from the linear dependence.

*Orbit width correction.*— The electric field which does work on curvature-drifting particles results from the field line motion that compresses plasmoids. It is natural then to consider that as particles gain energy from the Fermi acceleration process, the closed field lines they are bound to shrink in width:

$$\frac{dw}{dt} = -2\langle u_E \rangle_{pk}. \quad (3)$$

Here  $\langle u_E \rangle_{pk}$  is the *peak* value (not  $\delta$ -averaged) of  $u_E$  experienced by the particle as it transits *both* sides of the island (averaged between the left and right). This is generally slightly larger than  $\langle u_E \rangle_{\delta}$ , and we will assume that the ratio  $\langle u_E \rangle_{\delta} / \langle u_E \rangle_{pk} = \chi$  is approximately constant. We then substitute for  $\langle u_E \rangle_{\delta}$  in Eq.(2) allowing for the determination of  $w(\varepsilon_{\parallel})$ :

$$\frac{d\varepsilon_{\parallel}}{dw} = -2\chi \frac{\varepsilon_{\parallel}}{w}, \quad w = w_0 \left( \frac{\varepsilon_{\parallel}}{\varepsilon_{\parallel 0}} \right)^{-1/2\chi}, \quad (4)$$

leading to an enhanced power law acceleration rate:

$$\left( \frac{d\varepsilon_{\parallel}}{dt} \right)_{SF} \approx 4\chi \frac{\varepsilon_{\parallel 0}}{w_0} \langle u_E \rangle_{pk} \left( \frac{\varepsilon_{\parallel}}{\varepsilon_{\parallel 0}} \right)^{1+1/2\chi}. \quad (5)$$

The subscript ‘‘SF’’ has been added for ‘‘Super-Fermi’’, because the orbit-width correction exclusively leads to stronger energization over the linear expression. Additionally, although  $\chi$  is assumed to be constant it can vary somewhat due to minute details of the plasmoid structure. We will therefore make use of simulation data to provide a reasonable estimate. For ultra-relativistic particles which have  $v_{\parallel} \approx c$  (or  $\gamma \gg 1$ ), the super-Fermi acceleration rate is

$$\left( \frac{d\varepsilon_{\parallel}}{dt} \right)_{SF,UR} \approx 2\chi \frac{\varepsilon_{\parallel 0}}{w_0} \langle u_E \rangle_{pk} \left( \frac{\varepsilon_{\parallel}}{\varepsilon_{\parallel 0}} \right)^{1+1/\chi}. \quad (6)$$

where the change  $\varepsilon_{\parallel} \approx \gamma m_0 c^2$  is made but all other variables carry the same meaning [24]. Equation (6) indicates that the ultra-relativistic orbit-width power law correction is twice that of the non-relativistic version.

To verify Eq.(5), we evolved non-relativistic guiding-center test particles in time-dependent fields from a 2D compressible MHD resistive simulation of plasmoid reconnection. In the simulation, two similarly sized plasmoids grow at roughly the same rate and become nonlinear over several Alfvén crossing times of the simulation domain length  $L$ . Further details are available in the appendix. [34–36]. We also require a reasonable estimate for  $\chi$  in our plasmoids, so a single test particle was evolved inside a plasmoid for a time of  $L/v_A$ , and  $\langle u_E \rangle_{\delta} / \langle u_E \rangle_{pk}$  was calculated for 627 transits of the acceleration regions. An acceleration region is detected numerically as the time frame during which a particle experiences a  $\Delta\varepsilon_{\parallel}$  per time step of at least 25% of the maximum value during the same kick. This yielded a mean  $\chi$  of 0.75 ( $p = 1.67$  non-relativistically,  $p = 2.33$  ultra-relativistically), which will serve as our fiducial value henceforth.

An example test particle orbit is shown in Fig.2 with the initial fields that it experienced, for a total evolution time of  $t = 0.1L/v_A$ .  $\vec{u}_E$  is seen to be limited to a narrow central section of width roughly  $\delta$  which is approximately uniform, and peaks in magnitude at the reconnection outflow. In the following, we will refer to the effective plasmoid width  $w_p$  as the distance between the two maxima of  $u_E$ . The particle orbit shows a steady decrease in width  $w$  with no apparent change in  $h$  (given in Fig.1), also visible in the plot of  $\varepsilon_{\parallel}$  versus  $x$ -position. This particle was injected with an initial orbit width  $w_0 = 3w_p/4$  at  $t = 2.7L/v_A$ , roughly  $0.5L/v_A$  after the plasmoid became nonlinear. Calculating  $\dot{\varepsilon}_{\parallel}$  from Fig.2 and dividing by  $\langle u_E \rangle_{pk}(t, w)$ , the power law index  $p$  of the acceleration rate from the orbit width correction is 1.77.

To test Eq. (5) more broadly we performed a survey of simulations to calculate the particle acceleration rate power law with varying injection times and locations, shown in Fig.3. Test particles were injected into both

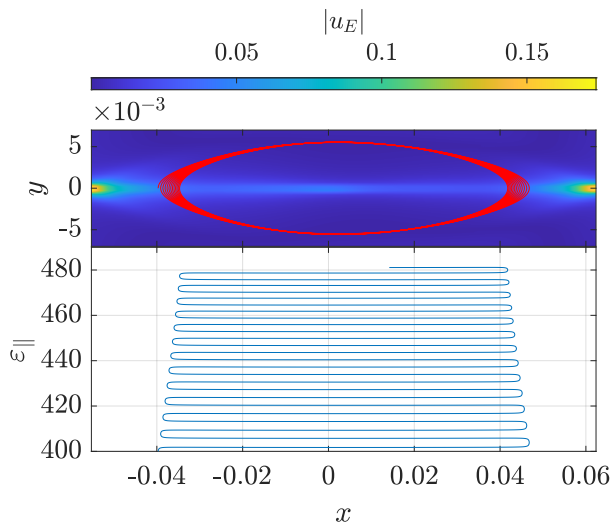


FIG. 2: Particle orbit path for injection at  $t = 2.7L/v_A$ , overlaid on initial magnitude of  $\bar{u}_E$ . Total time of integration is  $t = 0.1L/v_A$ .

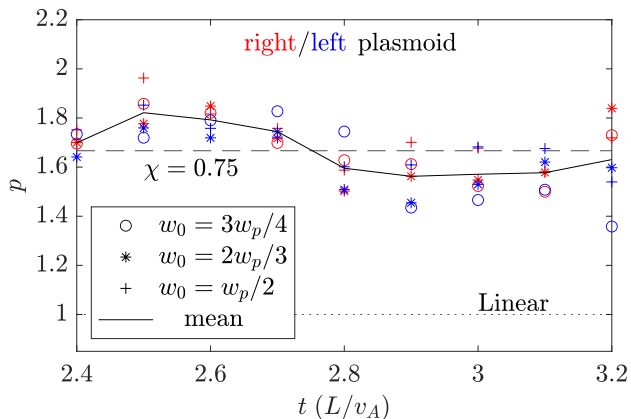


FIG. 3: Power law fits to test particle data for  $0.3L/v_A$  of evolution time, with the super-Fermi exponent assuming  $\chi = 0.75$ .

plasmoids, at 3 different initial orbit widths, and 9 different time steps in the MHD simulation. A total of 53 orbit-width corrected power law indices were calculated after  $0.3L/v_A$  of evolution time for each particle, excluding one particle which reached the center of its respective plasmoid before the end of the simulation. To remove the effect of the varying  $u_E$ , power laws are fit to  $\dot{\epsilon}_{\parallel}/\langle u_E \rangle_{pk}(t, w)$  to determine the index  $p$ , rather than just  $\dot{\epsilon}_{\parallel}$ . Both plasmoids are similar in size at each time step, therefore their power law indices are counted together, yet they can be distinguished by the color of their data points' markers. The fiducial power law  $p = 1.67$  predicted  $\chi = 0.75$  is shown as a black dashed line, while the linear Fermi prediction is shown as a black dotted line. The average measured power law agrees with the fiducial index to within 9% at all times, with a time-averaged  $p = 1.66$ . They also demonstrate importantly

that there is no net trend in the orbit-width corrected index  $p$  with the size of the plasmoid, which we will show not to be true when including the variation in  $\langle u_E \rangle_{pk}$ . Regardless of our choice of fiducial  $\chi$ , the expected lower limit on possible power law indices is 1.5, which is obeyed reasonably well, with a maximum  $p$  of 2 suggesting that  $\chi$  is generally at least 0.5. The fluctuations seen in our measured power law indices may be the result of weakly time dependent  $\chi$ , and/or imperfect separation of  $\langle u_E \rangle_{pk}$  from  $\dot{\epsilon}_{\parallel}$  numerically.

*Space- and time-varying  $\vec{E} \times \vec{B}$ .*—The effects of variation in  $\langle u_E \rangle_{pk}$  are much more dependent on the plasmoid structure and dynamics at the time of injection. Previous work has addressed the more circular core structure of large plasmoids through force balance [17], however we are concerned with the highly elongated outer region of the plasmoid. Without knowledge of the internal plasmoid structure, we have no analytical means by which to determine the modification to the acceleration rate power law by  $u_E$ . However, a trend in the behavior is identifiable through a survey of particle injection times when plasmoids possess a variety of sizes/fluxes. Here, we will investigate these effects specifically within the left plasmoid. In Fig.4, particles were injected with  $w_0 = 2w_p/3$ ,

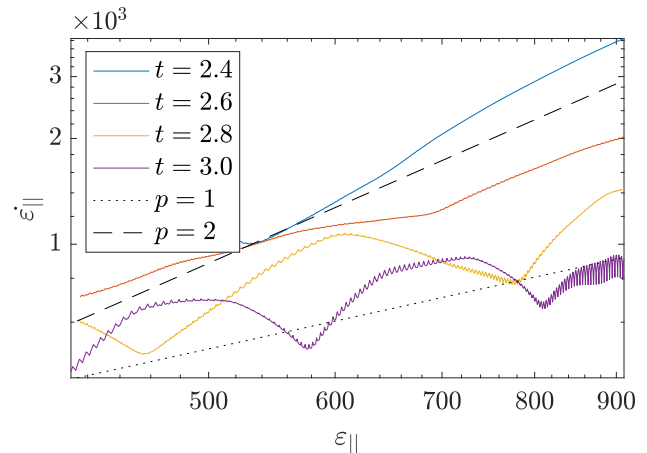


FIG. 4: Acceleration rates of test particles injected at various times throughout a plasmoid's life. Initial orbit width is  $w_0 = 2w_p/3$  for each time.

and all were evolved for at least  $0.5L/v_A$ . The trend in  $\dot{\epsilon}_{\parallel}$  demonstrates that as particles are injected later and later into a plasmoid, the effective power law index of their acceleration decreases. For nearly linear plasmoids the power law index can be larger than 2, while for large nonlinear plasmoids the power law index is able to drop below the linear Fermi rate. This variation occurs due to both the spatial and temporal dependence of  $\langle u_E \rangle_{pk}$ . The evolution of an  $x$ -slice of  $|u_E|$  within the reconnection layer for the left plasmoid is shown in Fig.5 [35]. Strong negative gradients are visible in the magnitude of  $u_E$  as one moves inward from the edges of the plasmoid. These gradients incorporate the relationship Eq.(4), and

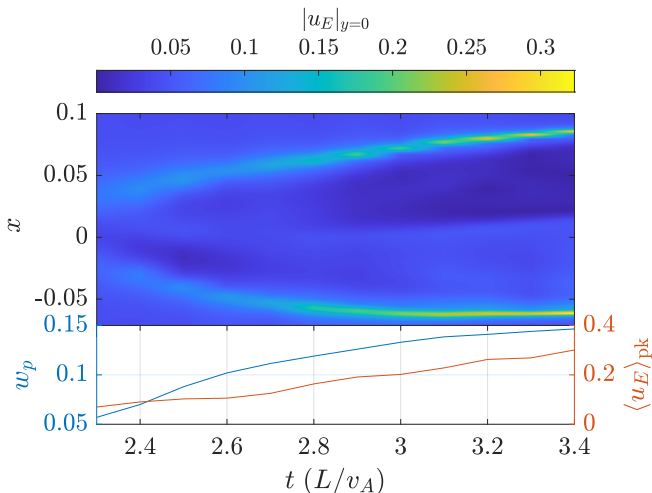


FIG. 5: Diagram of the evolution of the left plasmoid's  $|u_E|$  at  $y=1e-3$ , with  $\langle u_E \rangle_{pk}$  and  $w_p$  versus time highlighted below.

as a particle drifts inwards the field  $u_E$  that it experiences decreases, reducing the effective power law of the acceleration. These gradients become more pronounced as the plasmoid grows, further reducing the power law index of acceleration. The source of these gradients can be understood qualitatively through the conservation of mass, as the reconnection outflow expands into the plasmoid from the x-point. As a plasmoid grows, the area the outflow expands into becomes increasingly large, and therefore the inward gradient becomes more severe. Concurrently, the peak value of  $|u_E|$  grows with the size of the plasmoid. However, this is limited to the neighborhood of the outflow.

*Discussion.*—We have proposed that an enhanced Fermi acceleration process exists in 2D multiscale MHD reconnection. Results from analytical theory and test particle simulations suggest that a correction arises from changing magnetic island orbit widths for particles. This yields an acceleration rate power law relationship  $\dot{\epsilon}_{\parallel} \sim \epsilon_{\parallel}^{1.67}$  on average with the precise index varying somewhat due to island geometry, but generally remaining  $\sim 1.5$  or larger. To quantify the difference between linear and Super-Fermi acceleration, Fig.6 shows the ratio of the energy gain possible between the super- and linear Fermi models for a plasmoid of a given size, assuming  $\langle u_E \rangle_{pk}$  is constant for simplicity. Within each model, the total gain in energy  $\Delta\epsilon \doteq \epsilon_{\parallel}/\epsilon_{\parallel,0}$  is calculated for a particle which is allowed to drift inward until the island orbit width is  $w = 100\rho_L$ , where guiding center assumptions may weaken. In the linear Fermi calculation,  $w$  is fixed to  $w_p$ , while for Super-Fermi Eq.(4) is used. The ratio of the total gain between the models  $\Gamma \doteq \Delta\epsilon_{SF}/\Delta\epsilon_F$  is then shown as a function of the plasmoid size, here equivalent to the initial orbit width  $w_0$ . Consider the solar corona where  $\rho_{L,e} \sim 25$  cm, alongside the relevant length scales of a solar flare [37]. The length of the current sheet itself

is  $\sim 10^8\rho_{L,e}$ , meaning the limiting “monster” plasmoid size is still  $w_p \approx 10^{6-7}\rho_{L,e}$  [38, 39]. Even for some of the much smaller more populous plasmoids one would expect  $\Gamma > 10$ , and therefore substantial increase in energy gain over the linear Fermi model. In fact, given the asymptotic scalings  $\Gamma \sim (w_p/\rho_L)^{2\chi}$  and  $\Gamma_{UR} \sim (w_p/\rho_L)^{\chi}$ , numerous more reconnection conditions such as active galactic nuclei disks and magnetars would experience similar increases in the maximum possible energy gain [2].

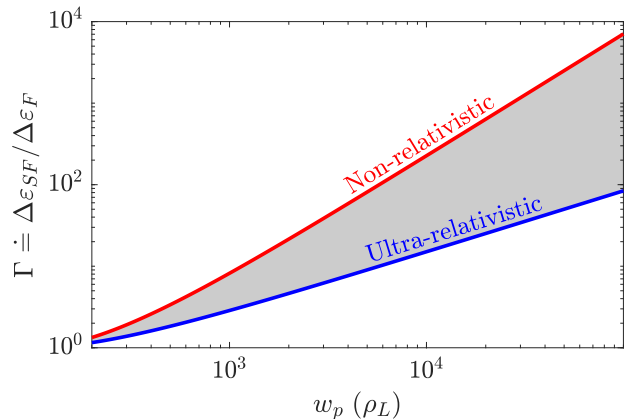


FIG. 6: Ratio of Super-Fermi to linear Fermi maximum possible total energy gain for a single plasmoid given  $w_p$ , assuming a particle can only drift inward until roughly  $w = 100\rho_L$ .

We additionally discussed the effects of the time-varying  $\vec{E} \times \vec{B}$  drift on the effective power law index, revealing a trend from high ( $\gtrsim 2$ ) to low ( $\lesssim 1$ ) power law indices as plasmoids get larger. In particular, this result places importance on the distribution of plasmoids in size and flux when investigating global particle energization in a multiscale current sheet [34, 38, 40, 41].

There are circumstances where the constant- $\chi$  assumption does not appear to hold, like early on during the linear phase of plasmoid growth or during mergers. In these situations,  $\chi$  in the left Eq.(4) will need to be considered more generally as  $\chi(w)$ , and the equation solved accordingly. For linear plasmoids, the average curvature rises rapidly as field lines move away from the x-point. This results in a knee-like feature in  $\dot{\epsilon}_{\parallel}$  with small but steeply rising initial acceleration that rapidly levels off. This also occurs near x-points in nonlinear plasmoids, but only represents a transient compared to the power law phase. Further generalization of this model would also be possible with development of a detailed understanding of the field and structure of plasmoid interiors as they grow [42]. Evolution of  $u_E$  introduces a time dependence which would lead to a separable O.D.E. for the energy as a function of time, and hence a way to refine the power law of  $\dot{\epsilon}_{\parallel}(\epsilon_{\parallel})$ . With knowledge of the spatial structure of these fields, Eq.(4) can once again be leveraged in directly modifying the power law. This would connect particle distributions to plasmoid distributions, possibly creating a route toward an analytical

description of multiscale reconnection energetic particle spectra [34, 43]. Additionally, one could account for the effects of a guide field in this model through the extension of various lengths out of the reconnection plane. The increase in radius of curvature and thus weakening of the curvature drift is countered exactly by an increase in path length in the acceleration region and hence energization time during a Fermi kick, leading to no change in  $\Delta\varepsilon_{\parallel}$ . On the other hand, the path length between Fermi kicks is extended to  $w \rightarrow w\sqrt{1 + (B_g/B_r)^2}$ , modifying the denominator of Eq. (2) accordingly. If  $B_g/B_r$  were roughly constant or varied slowly, the super-Fermi power law becomes  $p = 1 + \sqrt{1 + (B_g/B_r)^2}/2\chi$ , mirroring the steepening of power laws *and* weakening of acceleration set forth by Arnold et al [44]. Perhaps in most cases however, it may be required to consider  $B_g(w)/B_r(w)$  and integrate Eq.(4) exactly.

Certain reconnection conditions will require non-trivial adjustments to this model in order to appropriately be described by it. In kinetic plasmas, overlap with the model of Drake et al is expected, and particle motion is not so restricted to magnetic field lines, often due to  $\mu$  being poorly conserved. The lack of  $\mu$  conservation leads to *both*  $\varepsilon_{\parallel}$  and  $\varepsilon_{\perp}$  increasing during energization events [20]. Additionally, the Hall-effect field changes the direction of the curvature drift to be partially directed out of the plasmoid for *either* positive *or* negatively charged particles [18, 45, 46]. This could impede the inward motion of the gyro-center due to the  $\vec{E} \times \vec{B}$  drift, or even entirely reverse it as seen in Fig.2(b) of Drake et al (2006) [18], yielding an opposite-sign correction to the Fermi rate power law.

The data that support the findings of this study are available from the corresponding author upon reasonable request.

The authors thank Yi-Min Huang, Muni Zhou, and Nuno Loureiro for providing code and data for the MHD simulations, as well as Jim Drake, Fan Guo, and Matthew Kunz for helpful comments. This work was supported by NASA grant no. 80HQTR21T0060 and DoE Contract No. DE-AC02-09CH11466.

*Appendix on numerical simulation.*—To test Eq.(5), we performed guiding center simulations of test particles in a plasmoid reconnection scenario. To be precise,

we solved [24, 47]

$$\frac{d\vec{R}}{dt} = v_{\parallel}\hat{b} + \vec{u}_E \quad (7a)$$

$$\frac{dv_{\parallel}}{dt} = \frac{q}{m}E_{\parallel} + \vec{u}_E \cdot \left[ \left( v_{\parallel}\hat{b} + \vec{u}_E \right) \cdot \nabla\hat{b} \right] - \frac{\mu}{m}\hat{b} \cdot \nabla B, \quad (7b)$$

by an adaptive time step 2nd order-accurate midpoint method [48], using background data from an MHD simulation [35]. These equations have been simplified assuming that the time dependent drifts are weak due to the slow nature of the MHD background, and out-of-plane motion of the guiding center (not out-of-plane acceleration) is ignored given the 2D symmetry. Note also that in the simulation data used,  $E_{\parallel} = 0$ . An example snapshot of the simulation data is shown in figure 7. The adaptive

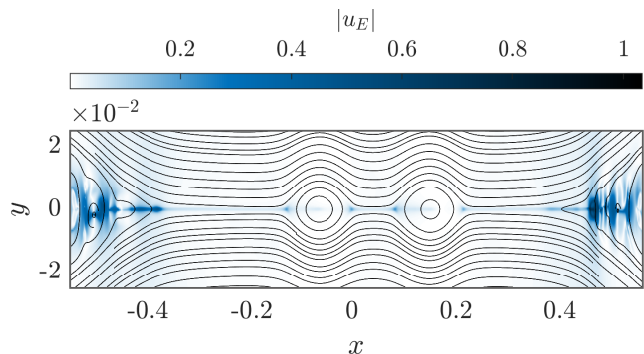


FIG. 7: Plot of full reconnecting current sheet in the simulation used, at  $t = 2.9L/v_A$ .  $|u_E| = E/B$  is shown with streamlines of the magnetic field overlaid.

time step is calculated as a fraction (CFL number) of the simulation grid cell-crossing time for the particle's velocity, and field interpolation from the grid to the particle's position/time is linear. In all calculations shown the CFL number is set to 0.1. The MHD simulation data used possesses a background plasma beta of  $\beta = 1$ , and a uniform Lundquist number of  $S = 10^5$ . Two plasmoids form, which eventually begin to merge at  $t = 3.6L/v_A$ , where  $L$  is the  $x$ -extent of the simulation domain [35]. The initial particle velocity is set to  $v_{\parallel} = 20v_A$  for the purpose of ensuring the small  $\Delta\varepsilon_{\parallel}$  approximations holds, however no significant difference was noticed in runs where the initial velocity was  $10v_A$  or  $5v_A$ . The perpendicular velocity of particles was set to  $v_{\perp} = v_A$  and generally plays little role unless  $v_{\perp} \sim v_{\parallel}$ , which leads to particle trapping at the island edge.

[1] M. Yamada, R. Kulsrud, and H. Ji, Magnetic reconnection, Rev. Mod. Phys. **82**, 603 (2010).

[2] H. Ji and W. Daughton, Phase diagram for magnetic reconnection in heliophysical, astrophysical, and labora-

- tory plasmas, *Phys. Plasmas* **18**, 111207 (2011).
- [3] H. Ji, W. Daughton, J. Jara-Almonte, A. Le, A. Stanier, and J. Yoo, Magnetic reconnection in the era of exascale computing and multiscale experiments, *Nat. Rev. Phys.* **4**, 263 (2022).
- [4] A. G. Emslie, B. R. Dennis, G. D. Holman, and H. S. Hudson, Refinements to flare energy estimates: A followup to “energy partition in two solar flare/cme events” by a. g. emslie et al., *J. Geophys. Res.* **110**, A11103 (2005).
- [5] S. Krucker, H. S. Hudson, L. Glesener, S. M. White, S. Masuda, J.-P. Wuelser, and R. P. Lin, Measurements of the Coronal Acceleration Region of a Solar Flare, *Astrophys. J.* **714**, 1108 (2010).
- [6] M. Øieroset, R. P. Lin, T. D. Phan, D. E. Larson, and S. D. Bale, Evidence for Electron Acceleration up to  $\sim 300$  keV in the Magnetic Reconnection Diffusion Region of Earth’s Magnetotail, *Phys. Rev. Lett.* **89**, 195001 (2002).
- [7] L.-J. Chen, N. Bessho, B. Lefebvre, H. Vaith, A. Asnes, O. Santolik, A. Fazakerley, P. A. Puhl-Quinn, A. Bhat-tacharjee, Y. Khotyaintsev, P. Daly, , and R. Torbert, (2009), “Multi-spacecraft observations of the electron current sheet, neighboring magnetic islands, and electron acceleration during magnetotail reconnection”, *Phys. Plasmas*, **16**, 056501, 2009.
- [8] O. V. Khabarova, G. P. Zank, G. Li, O. E. Malandraki, J. A. le Roux, and G. M. Webb, Small-scale magnetic islands in the solar wind and their role in particle acceleration. ii. particle energization inside magnetically confined cavities, *The Astrophysical Journal* **827**, 122 (2016).
- [9] L.-L. Zhao, G. P. Zank, O. Khabarova, S. Du, Y. Chen, L. Adhikari, and Q. Hu, An unusual energetic particle flux enhancement associated with solar wind magnetic island dynamics, *The Astrophysical Journal* **864**, 10.3847/2041-8213/aaddf6 (2018).
- [10] L.-L. Zhao, G. P. Zank, Y. Chen, Q. Hu, J. A. le Roux, S. Du, and L. Adhikari, Particle acceleration at 5 au associated with turbulence and small-scale magnetic flux ropes, *The Astrophysical Journal* **872**, 4 (2019).
- [11] S. Zenitani and M. Hoshino, The Generation of Nonthermal Particles in the Relativistic Magnetic Reconnection of Pair Plasmas, *Astrophys. J. Lett.* **562**, L63 (2001).
- [12] D. Uzdensky, Magnetic reconnection in extreme astrophysical environments (2011), published in *Space Sci. Rev.*, doi: 10.1007/s11214-011-9744-5.
- [13] A. Chien, L. Gao, S. Zhang, H. Ji, E. G. Blackman, W. Daughton, A. Stanier, A. Le, F. Guo, R. Follett, H. Chen, G. Fiksel, G. Bleotu, R. C. Cauble, S. N. Chen, A. Fazzini, K. Flippo, O. French, D. H. Froula, J. Fuchs, S. Fujioka, K. Hill, S. Klein, C. Kuranz, P. Nilson, A. Rasmus, and R. Takizawa, Direct measurement of non-thermal electron acceleration from magnetically driven reconnection in a laboratory plasma, *Nat. Phys.* , in press (2022), arXiv:https://arxiv.org/abs/2201.10052 [physics.plasm-ph].
- [14] J. Egedal, W. Daughton, and A. Le, Large-scale electron acceleration by parallel electric fields during magnetic reconnection, *Nature Physics* **8**, 321–324 (2012).
- [15] M. Hoshino, T. Mukai, T. Terasawa, and I. Shinohara, Suprathermal electron acceleration in magnetic reconnection, *J. Geophys. Res.* **106**, 25979 (2001).
- [16] D. Borovikov, V. Tenishev, T. I. Gombosi, S. E. Guidoni, C. R. DeVore, J. T. Karpen, and S. K. Antiochos, Electron acceleration in contracting magnetic islands during solar flares, *The Astrophysical Journal* **835**, 48 (2017).
- [17] H. Hakobyan, M. Petropoulou, A. Spitkovsky, and L. Sironi, Secondary energization in compressing plasmoids during magnetic reconnection, *The Astrophysical Journal* **912**, 48 (2021).
- [18] J. F. Drake, M. Swisdak, H. Che, and M. A. Shay, Electron acceleration from contracting magnetic islands during reconnection, *Nature* **443**, 553 (2006).
- [19] J. T. Dahlin, J. F. Drake, and M. Swisdak, The mechanisms of electron heating and acceleration during magnetic reconnection, *Phys. Plasmas* **21**, 092304 (2014).
- [20] F. Guo, H. Li, W. Daughton, and Y.-H. Liu, Formation of hard power laws in the energetic particle spectra resulting from relativistic magnetic reconnection, *Physical Review Letters* **113**, 10.1103/physrevlett.113.155005 (2014).
- [21] P. Montag, J. Egedal, E. Lichko, and B. Wetherton, Impact of compressibility and a guide field on fermi acceleration during magnetic island coalescence, *Phys. Plasmas* **24**, 062906 (2017), https://doi.org/10.1063/1.4985302.
- [22] E. G. Zweibel and M. Yamada, Magnetic reconnection in astrophysical and laboratory plasmas, *Annual Review of Astronomy and Astrophysics* **47**, 291–332 (2009).
- [23] L. Sironi and A. Spitkovsky, Relativistic reconnection: An efficient source of non-thermal particles, *The Astrophysical Journal* **783**, 10.1088/2041-8205/783/1/121 (2014).
- [24] B. Ripperda, O. Porth, C. Xia, and R. Keppens, Reconnection and particle acceleration in interacting flux ropes i. magnetohydrodynamics and test particles in 2.5d, *Monthly Notices of the Royal Astronomical Society* 10.1093/mnras/stx379 (2017).
- [25] A. Philippov, D. A. Uzdensky, A. Spitkovsky, and B. Cerutti, Pulsar radio emission mechanism: Radio nanoshots as a low-frequency afterglow of relativistic magnetic reconnection, *The Astrophysical Journal* **876**, 10.3847/2041-8213/ab1590 (2019).
- [26] F. Guo, Y.-H. Liu, W. Daughton, and H. Li, Particle acceleration and plasma dynamics during magnetic reconnection in the magnetically dominated regime, *Astrophys. J.* **806**, 1 (2015).
- [27] F. Guo, X. Li, W. Daughton, P. Kilian, H. Li, Y.-H. Liu, W. Yan, and D. Ma, Determining the dominant acceleration mechanism during relativistic magnetic reconnection in large-scale systems, *The Astrophysical Journal* **879**, 10.3847/2041-8213/ab2a15 (2019).
- [28] D. Ball, L. Sironi, and F. Özel, The mechanism of electron injection and acceleration in transrelativistic reconnection, *The Astrophysical Journal* **884**, 57 (2019).
- [29] H. Arnold, J. F. Drake, M. Swisdak, and J. Dahlin, Large-scale parallel electric fields and return currents in a global simulation model, *Physics of Plasmas* **26**, 102903 (2019).
- [30] F. Guo, Y.-H. Liu, X. Li, H. Li, W. Daughton, and P. Kilian, Recent progress on particle acceleration and reconnection physics during magnetic reconnection in the magnetically-dominated relativistic regime, *Physics of Plasmas* **27**, 080501 (2020).
- [31] X. Li, F. Guo, H. Li, A. Stanier, and P. Kilian, Formation of power-law electron energy spectra in three-dimensional low- $\beta$  magnetic reconnection, *The Astrophysical Journal* **884**, 118 (2019).
- [32] J. T. Dahlin, J. F. Drake, and M. Swisdak, Electron acceleration in three-dimensional magnetic reconnection with

- a guide field, *Physics of Plasmas* **22**, 100704 (2015).
- [33] T. Northrop, Sweet's mechanism for merging magnetic fields in conducting fluids, *Journal of Geophysical Research* **62**, 509 (1957).
- [34] Y.-M. Huang and A. Bhattacharjee, Distribution of plasmoids in high-lundquist-number magnetic reconnection, *Physical Review Letters* **109**, 10.1103/physrevlett.109.265002 (2012).
- [35] Y.-M. Huang and A. Bhattacharjee, Scaling laws of resistive magnetohydrodynamic reconnection in the high-lundquist-number, plasmoid-unstable regime, *Physics of Plasmas* **17**, 062104 (2010).
- [36] P. N. Guzdar, J. F. Drake, D. McCarthy, A. B. Hassam, and C. S. Liu, Three-dimensional fluid simulations of the nonlinear drift-resistive ballooning modes in tokamak edge plasmas, *Physics of Fluids B: Plasma Physics* **5**, 3712–3727 (1993).
- [37] B. Chen, C. Shen, D. E. Gary, K. K. Reeves, G. D. Fleishman, S. Yu, F. Guo, S. Krucker, J. Lin, G. M. Nita, and et al., Measurement of magnetic field and relativistic electrons along a solar flare current sheet, *Nature Astronomy* **4**, 1140–1147 (2020).
- [38] N. F. Loureiro, R. Samtaney, A. A. Schekochihin, and D. A. Uzdensky, Magnetic reconnection and stochastic plasmoid chains in high-lundquist-number plasmas, *Physics of Plasmas* **19**, 042303 (2012).
- [39] Y.-M. Huang and A. Bhattacharjee, Distribution of Plasmoids in High-Lundquist-Number Magnetic Reconnection, *Phys. Rev. Lett.* **109**, 265002 (2012).
- [40] L. Sironi, D. Giannios, and M. Petropoulou, Plasmoids in relativistic reconnection, from birth to adulthood: First they grow, then they go, *Monthly Notices of the Royal Astronomical Society* **462**, 48–74 (2016).
- [41] M. Zhou, N. F. Loureiro, and D. A. Uzdensky, Multi-scale dynamics of magnetic flux tubes and inverse magnetic energy transfer, *Journal of Plasma Physics* **86**, 10.1017/s0022377820000641 (2020).
- [42] S. Zenitani and T. Miyoshi, Plasmoid-dominated turbulent reconnection in a low-beta plasma, *The Astrophysical Journal* **894**, 10.3847/2041-8213/ab8b5d (2020).
- [43] S. Majeski, H. Ji, J. Jara-Almonte, and J. Yoo, Guide field effects on the distribution of plasmoids in multiple scale reconnection, *Physics of Plasmas* **28**, 092106 (2021).
- [44] H. Arnold, J. Drake, M. Swisdak, F. Guo, J. Dahlin, B. Chen, G. Fleishman, L. Glesener, E. Kontar, T. Phan, and et al., Electron acceleration during macroscale magnetic reconnection, *Physical Review Letters* **126**, 10.1103/physrevlett.126.135101 (2021).
- [45] J. F. Drake, M. A. Shay, and M. Swisdak, The hall fields and fast magnetic reconnection, *Phys. Plasmas* **15**, 042306 (2008).
- [46] L. Mal'ushkin, Model of hall reconnection, *Phys. Rev. Lett.* **101**, 225001 (2008).
- [47] T. Northrop, The guiding center approximation of charged particle motion, *Annals of Physics* **15**, 79 (1961).
- [48] W. H. Press, S. A. Teukolsky, W. T. Vetterling, and B. P. Flannery, *Numerical Recipes in C*, 2nd ed. (Cambridge University Press, Cambridge, USA, 1992).